Paper:

A Neural Adaptive Controller in Flapping Flight

Bo Cheng and Xinyan Deng

School of Mechanical Engineering, Purdue University
585 Purdue Mall, West Lafayette, Indiana 47907-2088, USA
E-mail: xdeng@purdue.edu

[Received February 2, 2012; accepted May 2, 2012]

In this paper, we propose a neural adaptive controller for attitude control in a flapping-wing insect model. The model is nonlinear and subjected to periodic force/torque generated by nominal wing kinematics. Two sets of model parameters are obtained from the fruit fly *Drosophila melanogaster* and the honey bee *Apis mellifera*. Attitude control is achieved by modifying the wing kinematics on a stroke-by-stroke basis. The controller is based on filtered-error with neural network models approximating system nonlinearities. Lyapunov-based stability analysis shows the asymptotic convergence of system outputs. We present simulation results for angular position stabilization and trajectory tracking. Trajectory tracking is illustrated by two cases: saccadic turning and sinusoidal variation in the yaw angle. The proposed controller successfully regulates flight orientation – roll, pitch and yaw angles – by generating desired torque resulting from tuning parameterized wing motion. Results furthermore show similarities between simulated and observed turning from real insects, suggesting some inherent properties in insect flight dynamics and control. The proposed controller has potential applications in future flapping-wing Micro Air Vehicles (MAVs).

Keywords: flapping flight, neural network, attitude control, Lyapunov stability, filtered error

1. Introduction

By subtly adjusting wing motion kinematics, insects are able to perform elaborate flight maneuvers and achieve fast stabilization of their body posture [1, 2]. It is challenging to study the control mechanisms adopted by insects for several reasons: first, the observation of insect flight behavior provides us with only a closed-loop view of the overall flight dynamics, and open-loop dynamics is hard to identify due to experimental limitations (e.g., [3, 4]). Second, it is difficult to capture the wing kinematics of insects in free flight, and studies on tethered flight are subject to many limitations [4]. Furthermore, flight control in insect relies heavily on the fast synthesis of different sensory information and occurs at both low-level sensory-motor reflex and high-level central nervous system [5–7]. Last, the unsteady aerodynamics of flapping flight is hard to model analytically [8].

With improvements in quasi-steady aerodynamic models and a variety of engineering tools (e.g., [9]), however, several simplified dynamic models of insect flight have been developed on a stroke-by-stroke basis [10–14]. Preliminary studies on flight control have, consequently, been carried out based on these models [15–18]. It has been shown, for example, that a linear optimal controller is sufficient to stabilize the body posture from perturbations [10]. An apparent limitation of this controller, however, is that it is only applicable to a linearized region near the hovering trim condition and cannot be used for tracking or maneuvering purposes. A nonlinear and adaptive controller for insect flight that is applicable to both position regulation and trajectory tracking is therefore of particular interest. The Neural Networks (NNs), with their *universal approximation property* [19, 20], are powerful paradigms for such purposes. They have been successfully applied to digital signal processing in open-loop applications such as classification and pattern recognition [20] and in closed-loop applications such as the control of robot manipulators [19].

The goal of this paper is to develop a neural adaptive controller for the nonlinear flapping-flight dynamics based on the quasi-steady aerodynamic model [10, 11, 21]. We focused our work on attitude dynamics because maintaining a desired body posture appears be to the primary goal of flight stabilization. This paper is organized as follows: Section 2 is a brief overview of the insect model used in the current work. Section 3 describes attitude dynamics, wing kinematic parameterization, filtered-error dynamics and the design of neural adaptive controller. Simulation results are summarized in Section 4. Conclusions and discussions on future works are presented in Section 5.

2. Insect Model

The insect body is modeled as a rigid object with three ellipsoids representing the head, thorax and abdomen, respectively (**Fig. 1**). The center of gravity is located below the wing base at distance l_1. Model parameters are obtained from the wing and body morphologies similar

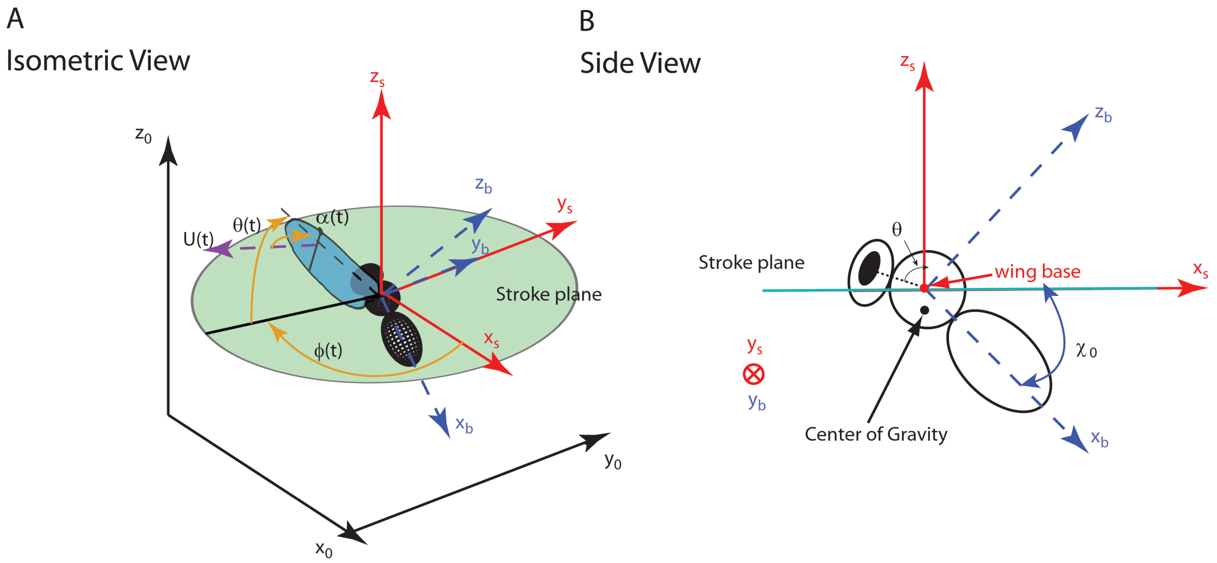

Fig. 1. A) An isometric view of the insect model in simulation: head, thorax and abdomen of the insect are modeled as ellipsoids. See **Table 1** for morphological data. Coordinate systems: the body frame (x_b, y_b and z_b), the inertial frame (x_0, y_0 and z_0) and the stroke-plane frame (x_s, y_s and z_s). All three frames have the same origin at the center of gravity of the fly. Wing kinematics are specified by three Euler angles – stroke angle (ϕ), deviation angle (θ) and rotation angle (ψ). Angle of attack (α) is defined as the angle between the wing chord and wing velocity. B) A side view: x_0 is the free body angle (desired pitch angle at hover) and θ represents the misalignment between the head and body.

to those of the fruit fly *Drosophila melanogaster* and the honey bee *Apis mellifera* (**Table 1**).

A complete model of closed-loop insect flight dynamics includes five subsystems: *aerodynamics*, *body dynamics*, *sensory systems*, *flight controller* and *actuator dynamics* (**Fig. 2**). A detailed description of a similar system is given in [10, 11]. Here, we briefly summarize the functions of each subsystem. Subsystem *aerodynamics* takes wing kinematics (stroke angle (ϕ) and rotation angle (ψ)) and their derivatives as inputs (elevation angle is not considered in this work) and generates corresponding instantaneous aerodynamic lift and drag forces (in the stoke-plane frame) as outputs. Lift and drag are calculated based on the quasi-steady aerodynamic model [8–10]. In the *force and torque generation process*, total wrench [22] in the body frame is obtained through a series of coordinate transformations from the stroke-plane frame to the body frame. By solving Newton-Euler equation for a rigid body [22], *rigid body dynamics* then calculates body kinematics – body position, velocity, orientation and angular velocity – based on stroke-averaged wrenches in the body frame. The *sensory system*, which takes inputs from various sensors (e.g., halters and ocelli), estimates the body kinematics and passes it to the *flight controller,* which generates appropriate control signals. In the current study, *sensory systems* and *actuator dynamics* are identical to those described in [11].

Table 1. Morphologies of the fruit fly *Drosophila melanogaster* and the honey bee *Apis mellifera.* Both insect models assume a horizontal stroke plane.

Species	Fruit fly *Drosophila*	Honey bee *Apis mellifera*
Mass m (mg)	1	93.8
Wing length R (mm)	2.4	9.52
Aspect ratio $\mathcal{AR}$	5.98	6.65
Body length L (mm)	2.5	15.4
Body width R (mm)	0.7	2.6
Dimensionless radius of the second moment of area r_2^2 (S)	0.35	0.3
Ratio of wing mass $\widehat{m}_W$ (%)	2.5	0.46
Flapping frequency n	212	197
Distance between wing base and center of gravity l_1 (mm)	0.65	4.0
Free body angle x_0 (degs)	45	56
Misalignment of the head w.r.t. body θ	$\frac{\pi}{6}$	$\frac{\pi}{6}$
Roll moment of inertia I_x (mg mm^2)	0.12	99.1
Pitch moment of inertia I_y	0.56	1935.2
Yaw moment of inertia I_z	0.56	1935.2

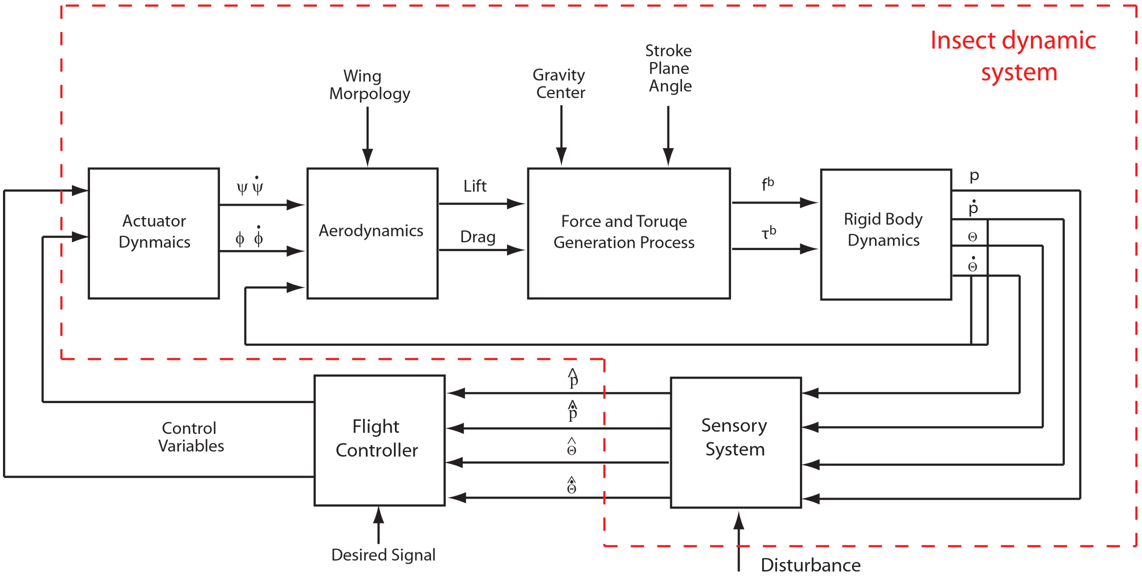

Fig. 2. Insect flight dynamic model: aerodynamics, body dynamics, sensory systems, flight controller and actuator dynamics. p and $\dot{p}$ represent body position and velocity. Θ and $\dot{\Theta}$ represent Euler angles for body orientation (roll, pitch and yaw) and their derivatives.

3. Attitude Dynamics and Neural Adaptive Control Design

3.1. Attitude Dynamics

The attitude dynamics of a rigid body is given by the Newton-Euler equation [11]:

$$I_b W\ddot{\Theta} + I_b\dot{W}\dot{\Theta} + W\dot{\Theta} \times I_b W\dot{\Theta} = \bar{\tau}_a^b \quad . \ . \ . \ . \quad (1)$$

where I_b is the body moment of inertia in the body frame, $\Theta = (\varphi, \theta, \phi)$ is a vector representing the three Euler angles (roll, pitch and yaw) specifying the body orientation and $\dot{\Theta}$ and $\ddot{\Theta}$ are its first and second derivatives. W is a transformation matrix that relates $\dot{\Theta}$ and $\ddot{\Theta}$ by $\omega_b = W\dot{\Theta}$. ω_b is the angular velocity in the body frame. $\bar{\tau}_a^b$ is stroke-averaged total aerodynamic torque in the body frame. Note that it has been shown in a previous study [2] that body rotational friction is negligible compared to the aerodynamic torque. Gravitational force has no effect on attitude dynamics. W is given by

$$W = \begin{bmatrix} 1 & 0 & -\sin\theta \\ 0 & \cos\phi & \cos\theta\sin\phi \\ 0 & -\sin\phi & \cos\phi\cos\theta \end{bmatrix} \quad . \ . \ . \ . \ . \ . \ . \quad (2)$$

Defining $I_b W = M(\Theta)$, $I_b\dot{W} = V(\Theta, \dot{\Theta})$, and $\sigma(\Theta, \dot{\Theta}) = W\dot{\Theta} \times I_b W\dot{\Theta}$, the equation can be written in a form similar to that for robot manipulator dynamics [19]:

$$M(\Theta)\ddot{\Theta} + V(\Theta, \dot{\Theta})\dot{\Theta} + \sigma(\Theta, \dot{\Theta}) = \bar{\tau}_a^b \quad . \ . \ . \quad (3)$$

where cross product $\sigma(\Theta, \dot{\Theta})$ is viewed as a disturbance term in subsequent controller design (it is expected to be negligible compared to the other terms). Next, for convenience in proving controller stability, we further rewrite the equation to an alternative form:

$$M(\ddot{\Theta}) + V_m\dot{\Theta} + \sigma(\Theta, \dot{\Theta}) = \bar{\tau}_a^b \ . \ . \ . \ . \ . \ . \ . \ . \quad (4)$$

where $M - V_m$ is designed to be a screw symmetric matrix while keeping $V_m\dot{\Theta} = V\dot{\Theta}$. To calculate the nine unknowns in the matrix V_m, two conditions must be satisfied [19]:

1) $\dot{M} - 2V_m$ is skew symmetric.

2) $V_m\dot{\Theta} = V\dot{\Theta}$.

1) and 2) provide nine linearly independent equations for the nine unknowns, thereby guarantee a unique solution. Note that the exact solution is not required in the controller design or the proof of stability.

3.2. Wing Kinematics Parameterization

Wing kinematics and flight characteristics vary among different flying animals, as do the unsteady aerodynamic mechanisms adapted [23]. Some common strategies for modulating wing motion could, however, still be identified in both free and tethered flight [24]. It has been shown in simulation that by a proper parameterization of wing kinematics, aerodynamic torque acting on the three orthogonal body axes and vertical force can be controlled almost independently in a linear fashion, although there exists unavoidable coupling between longitudinal and lateral dynamics [10, 25]. In this study, wing kinematics is parameterized by three parameters $(\gamma, \alpha_l, \alpha_r)$ denoted as vector v for 3DOF attitude dynamics (the system is expected to be fully actuated). Mathematically, the wing kinematics is written as [26]:

$$\begin{aligned} \phi_l(t) &= g_\phi(t) + \gamma g_1(t) \\ \phi_r(t) &= g_\phi(t) - \gamma g_1(t) \\ \psi_l(t) &= g_\psi(t) + \alpha_l g_2(t) \\ \psi_r(t) &= g_\psi(t) + \alpha_r g_2(t) \end{aligned} \quad . \ . \ . \ . \ . \ . \ . \ . \ . \ . \quad (5)$$

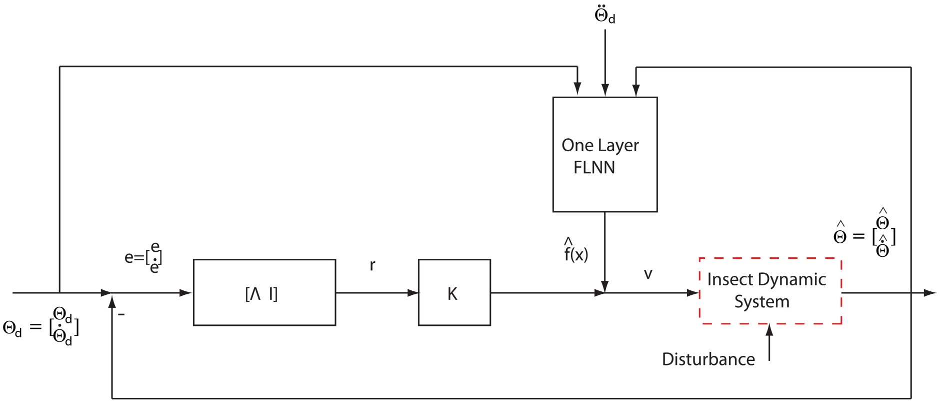

Fig. 3. A schematic diagram of the controller structure.

where $g_\phi(t)$, $g_\psi(t)$, $g_1(t)$ and $g_2(t)$ are period functions defined as:

$$
\begin{aligned}
g_\phi(t) &= \frac{\pi}{3}\cos\left(\frac{2\pi}{T}t\right)\\
g_\psi(t) &= \frac{\pi}{4}\sin\left(\frac{2\pi}{T}t\right)\\
g_2(t) &= \left(0.3\sin\left(\frac{\pi}{T}t\right) - 0.1\sin\left(\frac{3\pi}{T}t\right)\right)\\
&\quad \operatorname{sign}\left(\sin\frac{\pi}{T}t\right)\\
g_2(t) &= g_1(t) \quad \ldots\ldots\ldots\ldots\ldots (6)
\end{aligned}
$$

where γ represents the difference in stroke angles between the left and right wings. α_l and α_r are designed to modulate the timing and magnitude of wing rotation. Mapping $\mathscr{A}(\cdot)$ from the above wing parameters ($v \in \mathbb{R}^3$) to the mean aerodynamic torque ($\bar{\tau}_a^b \in \mathbb{R}^3$) is a complex nonlinear function. Affine approximation can be obtained, however, by solving a Least-Square (LS) problem [27]. Specifically, we randomly select wing parameters $(\gamma, \alpha_l, \alpha_r)$, each of which has a value between $[-1, 1]$, and calculate the corresponding aerodynamic torque $\bar{\tau}_a^b$ in the body frame via simulation. The v and $\bar{\tau}_a^b$ pairs are used to solve the LS problem:

$$\bar{\tau}_a^b = \pi_0 + \Pi v + \delta(v) \quad \ldots\ldots\ldots\ldots (7)$$

where $\pi_0 \in \mathbb{R}^3$ and $\Pi \in \mathbb{R}^{3\times 3}$ are unknowns to be solved and $\delta(v)$ is approximation error. Eq. (7) is then used to estimate stroke-averaged torque $\bar{\tau}_a^b$ from v, which is considered to be the control input for producing the desired wing motion that achieves attitude regulations.

3.3. Filtered-Error-Based Control with a Neural Network

In this section, we present a filtered-error-based control paradigm with a NN approximating the nonlinear function in the system dynamics (NN design and proof of its stability are discussed in the next section).

First, we define the tracking error $e(t)$ and filtered tracking error $r(t)$ as:

$$
\begin{aligned}
e &= \Theta_d - \Theta\\
r &= \dot{e} + \Lambda e \quad \ldots\ldots\ldots\ldots\ldots (8)
\end{aligned}
$$

where Θ_d is the desired angular position. Λ is a positive-definite design matrix that is properly selected to ensure the stability of the system. Taking the derivative of r, multiplying M on both sides, and incorporating Eq. (4), we have:

$$
\begin{aligned}
M\dot{r} &= M(\ddot{\Theta}_d + \Lambda\dot{e}) + V_m(\dot{\Theta}_d + \Lambda e)\\
&\quad - V_m r - \bar{\tau}_a^b + \sigma(\Theta, \dot{\Theta})\\
&= -V_m r + f(x) + \sigma(\Theta, \dot{\Theta}) - \bar{\tau}_a^b \quad \ldots\ldots (9)
\end{aligned}
$$

where $f(x) = M(\ddot{\Theta}_d + \Lambda\dot{e}) + V_m(\dot{\Theta}_d + \Lambda e)$ is the nonlinear function to be approximated by NN, and

$$x = \begin{bmatrix} e \\ \dot{e} \\ \Theta_d \\ \dot{\Theta}_d \\ \ddot{\Theta}_d \end{bmatrix} . \quad \ldots\ldots\ldots\ldots\ldots (10)$$

As stated above, we consider $\sigma(\Theta, \dot{\Theta})$ to be a bounded disturbance term. Here, Eq. (9) is referred as filtered-error dynamics.

A NN-approximation-based controller with an outer PD tracking loop is derived by setting the desired control torque as:

$$\bar{\tau}_{db}^{a} = \hat{f}(x) + Kr \quad \ldots\ldots\ldots\ldots (11)$$

where $\hat{f}(x)$ is the approximation of $f(x)$ using a *one-layer Functional-Link Neural Network* (FLNN) [19], detailed in the next section. **Fig. 3** shows a schematic diagram of the control loop structure. Note that $Kr = K(\dot{e} + \Lambda e)$ functions as a PD controller with two design parameters, K and Λ. Next, according to Eqs. (7) and (11), we calculate the control input (wing kinematic parameters) as:

$$v = \Pi^{-1}\left(\hat{f}(x) + Kr - \pi_0\right). \quad \ldots\ldots\ldots (12)$$

Due to the error $\sigma(v)$ in the linear mapping for aerodynamic torque (Eq. (7)), the difference between desired and actual torque is:

$$\tilde{\bar{\tau}}_a^b = \bar{\tau}_{db}^a - \bar{\tau}_a^b = \hat{f}(x) + Kr - \mathscr{A}(v). \quad . \ . \ . \ (13)$$

Filtered-error dynamics therefore becomes:

$$\begin{aligned} M\dot{r} &= -V_m r + f(x) + \sigma(\Theta,\dot{\Theta}) - \bar{\tau}_a^b \\ &= \tilde{f}(x) - (V_m + K)r + \sigma(\Theta,\dot{\Theta}) + \tilde{\bar{\tau}}_a^b \quad . \ . \ (14) \end{aligned}$$

where $\tilde{f}(x) = f(x) - \hat{f}(x)$ is approximation error by FLNN. $\tilde{\bar{\tau}}_a^b$ and $\sigma(\Theta,\dot{\Theta})$ are both considered to be disturbances.

3.4. Partitioned One-Layer Functional-Link Neural Network Design

The problem then remains to design the NN and to prove its stability. We chose a one-layer FLNN to approximate $f(x)$ because of its simplicity and linear weight-updating algorithm. Its universal approximation property, however, holds only if its generalized activation function, $\phi(x)$, is selected as a *basis set* [19]. That is, for any function $f(x)$ defined in a compact, simply connected set of $S \in \mathbb{R}^n$, there exist weights W such that:

$$f(x) = W^T\phi(x) + \varepsilon \quad . \ . \ . \ . \ . \ . \ . \ . \ . \ . \ . \ (15)$$

where ε is estimation error with a known bound ε_N dependent on region S. Activation function $\phi(x)$ is a predetermined *basis* function set that represents a mapping from the input of FLNN to the output of its hidden layer [19]. W represents the second layer of weights. Note that the one-layer FLNN has one layer of adjustable weights and two layers of neurons (**Fig. 4**).

The selection of the *basis* function set is not unique. In our specific problem, the basis set is constructed by partitioning the NN into subnets that approximate each term in $f(x)$ separately (**Fig. 4**):

$$\begin{aligned} M(\ddot{\Theta}_d + \Lambda\dot{e}) &= \tilde{W}_M^T\phi_M(x) + \varepsilon_M \\ V_m(\dot{\Theta}_d + \Lambda e) &= \tilde{W}_V^T\phi_V(x) + \varepsilon_V. \quad . \ . \ . \ . \ (16) \end{aligned}$$

The sum of these two subsets is the output of the FLNN. The filtered-error dynamics given by Eq. (14) then becomes

$$\begin{aligned} M\dot{r} = {} & \tilde{W}_M^T\phi_M(x) + \tilde{W}_V^T\phi_V(x) - (V_m + K)r \\ & + \sigma(\Theta,\dot{\Theta}) + \tilde{\bar{\tau}}_a^b + \varepsilon_M + \varepsilon_V \quad . \ . \ . \ . \ . \ (17) \end{aligned}$$

where ε_M and ε_V are estimation errors for M and V_m. $\tilde{W}_M^T$ and $\tilde{W}_V^T$ are the adjustable weights for the two subnets.

Next, the weight-tuning algorithm is given by the theorem below to ensure the stability of the closed-loop system.

Assume that the desired trajectory Θ_d is bounded by Θ_B and initial tracking error $r(0)$ satisfies the initial condition assumption [19]. Let the NN construction error be bounded by $\varepsilon_{MN} + \varepsilon_{VN}$, system identification error $\tilde{\bar{\tau}}_a^b$ bounded by τ_B, and $\sigma(\Theta,\dot{\Theta})$ bounded by σ_B. In the filtered-error dynamics (Eq. (17)), let the gain K satisfy:

$$K_{\min} > \frac{(\varepsilon_{MN} + \varepsilon_{VN} + \sigma_B + \tau_B)(c_0 + c_2)}{b_x - \Theta_B} \quad . \ . \ . \ (18)$$

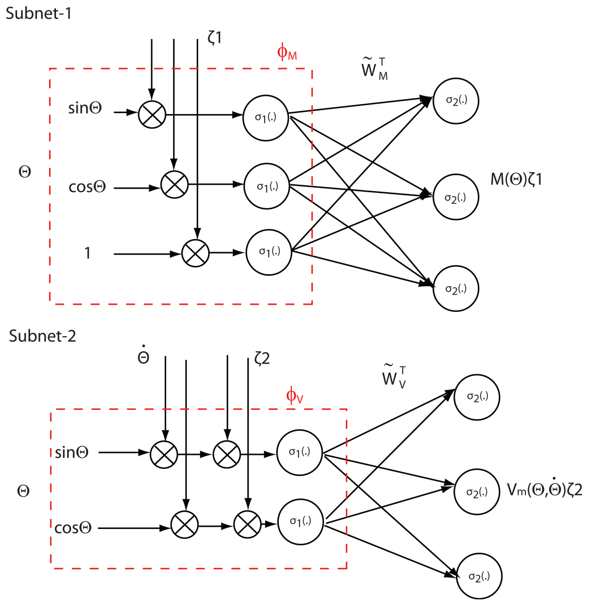

Fig. 4. A schematic view of the partitioned FLNN: subnet-1 and 2 approximating $M(\Theta)\zeta_1$ and $V_m(\Theta,\dot{\Theta})\zeta_2$, respectively, where $\zeta_1 = \ddot{\Theta}_d + \Lambda\dot{e}$ and $\zeta_2 = \dot{\Theta}_d + \Lambda e$. Hidden layer activation function $\sigma_1(\cdot)$ is selected as a symmetric sigmoid function. Output layer activation function $\sigma_2(\cdot)$ is selected as a pure linear function. Subnet-1 consists of 21 hidden layer neurons and 3 output layer neurons. Subnet-2 consists of 72 hidden layer neurons and 3 output layer neurons.

where $K_{\min}$ is the minimum singular value of K. $S_x \equiv \{x|\|x\| < b_x\}$ is the compact set that NN approximation holds and c_0 and c_2 are two positive constants (explained later). It is shown that, given weight tuning:

$$\begin{aligned} \dot{\hat{W}}_M &= F_M\phi_M(x)r^T, \\ \dot{\hat{W}}_V &= F_V\phi_V(x)r^T, \quad . \ . \ . \ . \ . \ . \ . \ . \ . \ . \ . \ (19) \end{aligned}$$

with constant design parameter matrices $F_i = F_i^T > 0$ $(i = M, V)$, and assume that the hidden-layer output $\phi_i(x)$ is Persistence of Excitation (PE) [19]; then the filtered-tacking error $r(t)$ is *Uniformly Ultimately Bounded* (UUB) [19], and NN weight estimates $\hat{W}_i$ $(i = M, V)$ are bounded.

In the following, we give a detailed derivation of partitioned NN weight tuning and proof of boundedness. The derivation is adapted from [19], with additional modifications, to our specific problem.

Let the NN approximation property $f_i(x) = W_i^T\phi_i(x) + \varepsilon_i$ $(i = M, V)$ hold for each term in function $f(x)$ (Eq. (9)), with given accuracy ε_{MN} and ε_{VN} for all x in the compact set $S_x \equiv \{x|\|x\| < b_x\}$ with $b_x > \Theta_B$. Define $S_r \equiv \{r|\|r\| < (b_x - q_B)/(c_0 + c_2)\}$, where c_0 and c_2 are two positive constants determined by design matrix Λ and initial tracking error e_0 (for definitions, see p. 178 of [19]). Let $r(0) \in S_r$, the approximation property then holds.

Define the Lyapunov function candidate:

$$L = \frac{1}{2}r^T M r + \frac{1}{2}tr(\tilde{W}_M^T F_M^{-1}\tilde{W}_M + \tilde{W}_V^T F_V^{-1}\tilde{W}_V). \quad (20)$$

Differentiating yields:

$$\dot{L} = r^T M\dot{r} + \frac{1}{2} r^T \dot{M} r + tr\left\{(\tilde{W}_M^T F_M^{-1} \dot{\tilde{W}}_M + \tilde{W}_V^T F_V^{-1} \dot{\tilde{W}}_V)\right\}. \quad . \quad (21)$$

Substitute $M\dot{r}$ from the filtered-error dynamics (Eq. (17))

$$\begin{aligned}\dot{L} &= r^T \left\{\tilde{W}_M^T \phi_M(x) + \tilde{W}_V^T \phi_V(x) + \varepsilon_M + \varepsilon_V \right.\\ &\qquad \left. -(V_m + K)r + \sigma(\Theta,\dot{\Theta}) + \tilde{\tilde{\tau}}_a^b\right\}\\ &\quad + \frac{1}{2} r^T \dot{M} r + tr\langle(\tilde{W}_M^T F_M^{-1} \dot{\tilde{W}}_M + \tilde{W}_V^T F_V^{-1} \dot{\tilde{W}}_V)\rangle\\ &= -r^T K r + \frac{1}{2} r^T (\dot{M} r - 2V_m) r\\ &\quad + tr\left\{\tilde{W}_M^T (F_M^{-1} \dot{\tilde{W}}_M + \phi_M(x) r^T) \right.\\ &\qquad \left. + \tilde{W}_V^T (F_V^{-1} \dot{\tilde{W}}_V + \phi_V(x) r^T)\right\}\\ &\quad + r^T (\varepsilon_M + \varepsilon_V + \sigma(\Theta,\dot{\Theta}) + \tilde{\tilde{\tau}}_a^b). \quad . \quad . \quad . \quad (22)\end{aligned}$$

The second term is zero due to the screw-symmetric property and the third term is zero if we select:

$$\begin{aligned}\dot{\tilde{W}}_M &= -F_M \phi_M(x) r^T,\\ \dot{\tilde{W}}_V &= -F_V \phi_V(x) r^T. \quad . \quad . \quad . \quad . \quad . \quad . \quad . \quad . \quad . \quad . \quad . \quad (23)\end{aligned}$$

Because $\tilde{W}_i = W_i - \hat{W}_i$ $(i = M, V)$ and W_i is constant, we have the weight-updating law:

$$\begin{aligned}\dot{\hat{W}}_M &= F_M \phi_M(x) r^T,\\ \dot{\hat{W}}_V &= F_V \phi_V(x) r^T. \quad . \quad . \quad . \quad . \quad . \quad . \quad . \quad . \quad . \quad . \quad . \quad (24)\end{aligned}$$

Now,

$$\begin{aligned}\dot{L} &= -r^T K r + r^T (\varepsilon_M + \varepsilon_V + \sigma(\Theta,\dot{\Theta}) + \tilde{\tilde{\tau}}_a^b)\\ &\leq -K_{\min}\|r\|^2 + (\varepsilon_{MN} + \varepsilon_{VN} + \sigma_B + \tau_B)\|r\| \quad (25)\end{aligned}$$

with $K_{\min}$ the minimum singular value of K. Since $(\varepsilon_{MN} + \varepsilon_{VN} + \sigma_B + \delta_B)$ is constant, $\dot{L} \leq 0$ if:

$$\|r\| > \frac{\varepsilon_{MN} + \varepsilon_{VN} + \sigma_B + \delta_B}{K_{\min}} \equiv b_r \quad . \quad . \quad . \quad . \quad . \quad (26)$$

Selecting the gain based on the above equation ensures that the compact set defined by $\|r\| \leq b_r$ is contained in S_r so that the approximation property holds. Tracking error $r(t)$ is therefore bounded and continuity results in the boundedness of $\dot{r}(t)$.

Next, we prove the boundedness of $\hat{W}_M$ and $\hat{W}_V$. It is easy to see that the NN output:

$$\begin{aligned}y &= \tilde{W}_M^T \phi_M(x) + \tilde{W}_V^T \phi_V(x)\\ &= M\dot{r} + (V_m + K)r - \sigma(\Theta,\dot{\Theta}) - \tilde{\tilde{\tau}}_a^b - \varepsilon_M - \varepsilon_V \quad (27)\end{aligned}$$

is bounded. Therefore, the NN weight-error dynamics are given by

$$\begin{aligned}\dot{\tilde{W}}_M &= -F_M \phi_M r^T\\ \dot{\tilde{W}}_V &= -F_V \phi_V r^T\\ y^T &= \phi_M^T \tilde{W}_M + \phi_V^T \tilde{W}_V \quad . \quad . \quad . \quad . \quad . \quad . \quad . \quad . \quad . \quad . \quad (28)\end{aligned}$$

with $y(t)$ and $r(t)$ bounded. Using Kronecker product $\otimes$, we write the above equations into a uniform vector form:

$$\begin{aligned}\frac{d}{dt}\begin{bmatrix} vec(\dot{\tilde{W}}_M) \\ vec(\dot{\tilde{W}}_V) \end{bmatrix} &= -\begin{bmatrix} I \otimes F_M \phi_M \\ I \otimes F_V \phi_V \end{bmatrix} \begin{bmatrix} r \\ r \end{bmatrix}\\ y^T &= ([I \otimes \phi_M^T \quad I \otimes \phi_V^T]) \begin{bmatrix} vec(\tilde{W}_M) \\ vec(\tilde{W}_V) \end{bmatrix} \quad . \quad . \quad . \quad (29)\end{aligned}$$

where the $vec(A)$ operator stacks the columns of a matrix A to form a vector. The assumption of the PE condition for ϕ_M^T and ϕ_V^T guarantees the PE condition of $[I \otimes \phi_M^T \quad I \otimes \phi_V^T]$ and thus the uniform complete observability of this system. According to Lemma 4.2.1 in [19], the boundedness of $y(t)$ and $r(t)$ assures the boundedness of $\begin{bmatrix} vec(\dot{\tilde{W}}_M) \\ vec(\dot{\tilde{W}}_V) \end{bmatrix}$ and hence, of $\hat{W}_M$ and $\hat{W}_V$.

Table 2. Values of controller parameters.

Morphology	Λ	K	F_M	F_V
Fruit fly *Drosophila*	18	2.8×10^{-4}	10^{-4}	10^{-4}
Honey bee *Apis mellifera*	30	5	0.1	0.1

Collectively, the stability of the system and the boundedness of NN weights are ensured from the above theorem with a proper selection of design parameters. These parameters include filtered-error design matrix Λ, PD control gain, and NN learning constants F_M and F_V, properly selected with respect to the morphologies of the fruit fly and the honey bee.

4. Simulation Results

The controller was finally tested using the flight dynamic model described in Section 2. **Table 2** lists the values of design parameters Λ, K, F_M and F_V. For both the fruit fly and the honey bee models, initial body orientation was set at $\Theta_0 = [0,0,0]^T$, with body frame aligned with the inertial frame. The model insects were controlled to follow two types of angular trajectories: 1) saccadic-like turning and 2) sinusoidal variation in the yaw angle.

4.1. Hovering and Tracking of Angular Positions

In the first simulation, model insects were first controlled to maintain a desired body posture at hovering. Then, at 100 ms, they were controlled to perform an abrupt turn about the vertical yaw axis.

Simulation results are summarized for the fruit fly model in **Fig. 5**. The controller successfully achieved the hovering stabilization and the tracking task. Specifically, the fruit fly first produced large nose-up torque to reach the desired body posture at 45° pitch angle (free body an-

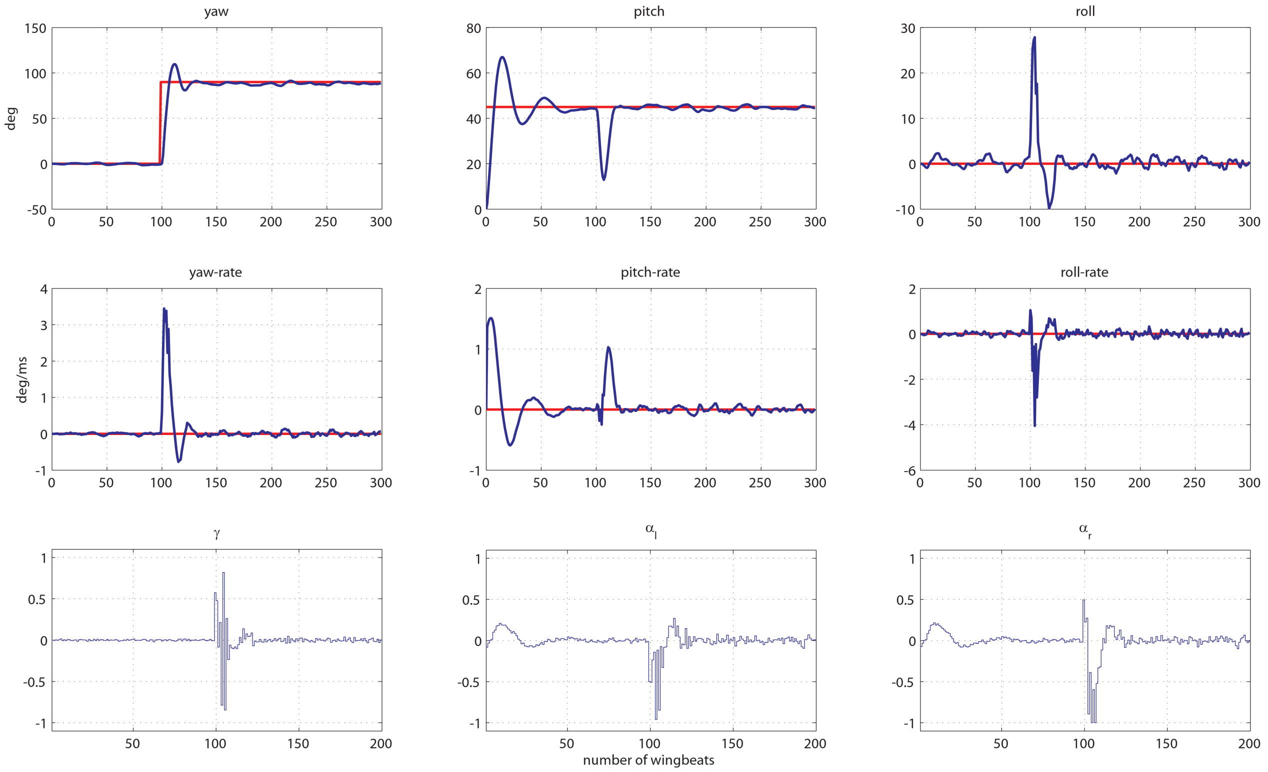

Fig. 5. Tracking saccadic turning in the fruit fly model.

gle). At 100 ms, the fly performed a banked turn with a nose-down motion (positive roll angle and decrease in pitch angle in **Fig. 5**) and maintained hovering afterwards. Note that this simulated turning demonstrated body movement similar to that observed in free insect flight [2], which may suggest some inherent properties of the maneuvers in flapping flight, such as coupling between the yaw and roll torques.

Using the design parameters in **Table 2** for the honey bee model, the system output $\Theta(t)$ was poorly convergent but bounded (results not shown). We noted that the poor performance is largely due to the oscillation about the roll axis. This is not surprising if we look at the body moment of inertia matrix. The ratio I_x/I_z is less than $1/20$ ($1/5$ for the fruit fly), indicating a relatively low roll moment of inertia. The roll and yaw torques were, however, of the same order of magnitude because they were coupled, so the acceleration about the roll axis was much larger than that about the yaw axis, possibly leading to the oscillation. This problem can be solved, however, if we modify the matrix Π as follows:

$$\Pi' = \begin{bmatrix} 9 & 0 & 0 \\ 0 & 1 & 0 \\ 0 & 0 & 1 \end{bmatrix} \Pi. \quad \ldots\ldots\ldots\ldots \quad (30)$$

When the first row of Π is magnified, the controller predicts greater roll torque than that actually produced. This in turn reduces the control input and changes the relative ratio between the roll and yaw torques produced. Corresponding simulation results are summarized in **Fig. 6**. The modified controller successfully achieved the hovering stabilization and the tracking tasks. Similar to the case of the fruit fly, a banked turn with nose-down motion was observed. However, there were some differences, for example, a large roll tilting toward the direction opposite to the banking was observed (large negative roll angle in **Fig. 6**). In addition, note that the honey bee had much higher control input v than the fruit fly. This suggests that the honey bee requires a higher wing kinematic asymmetry to perform a maneuver, which is consistent with the observations from real flight [2, 28].

In the next simulation, model insects were controlled to follow sinusoidal yaw variation starting at 50 ms. Results are summarized in **Figs. 7** and **8** for the fruit fly and the honey bee, respectively. For both models, tracking was successfully achieved with little phase delay. The oscillation of the yaw angle was accompanied by oscillations in the roll and pitch angles. In particular, the tracking was accomplished by a series of syn-directional banking motions.

4.2. NN and PD Control

As mentioned previously, the current controller is the combination of a PD controller and a NN approximating nonlinear terms. However, it is surprising to note, that setting the design parameter K to zero, or even negative, the above tracking tasks can be still successfully achieved if F_M and F_V are properly selected (values not shown). This indicates that Eq. (18) is a sufficient, but not a necessary condition and the NN itself can function as a controller without PD control. Furthermore, we found that as long

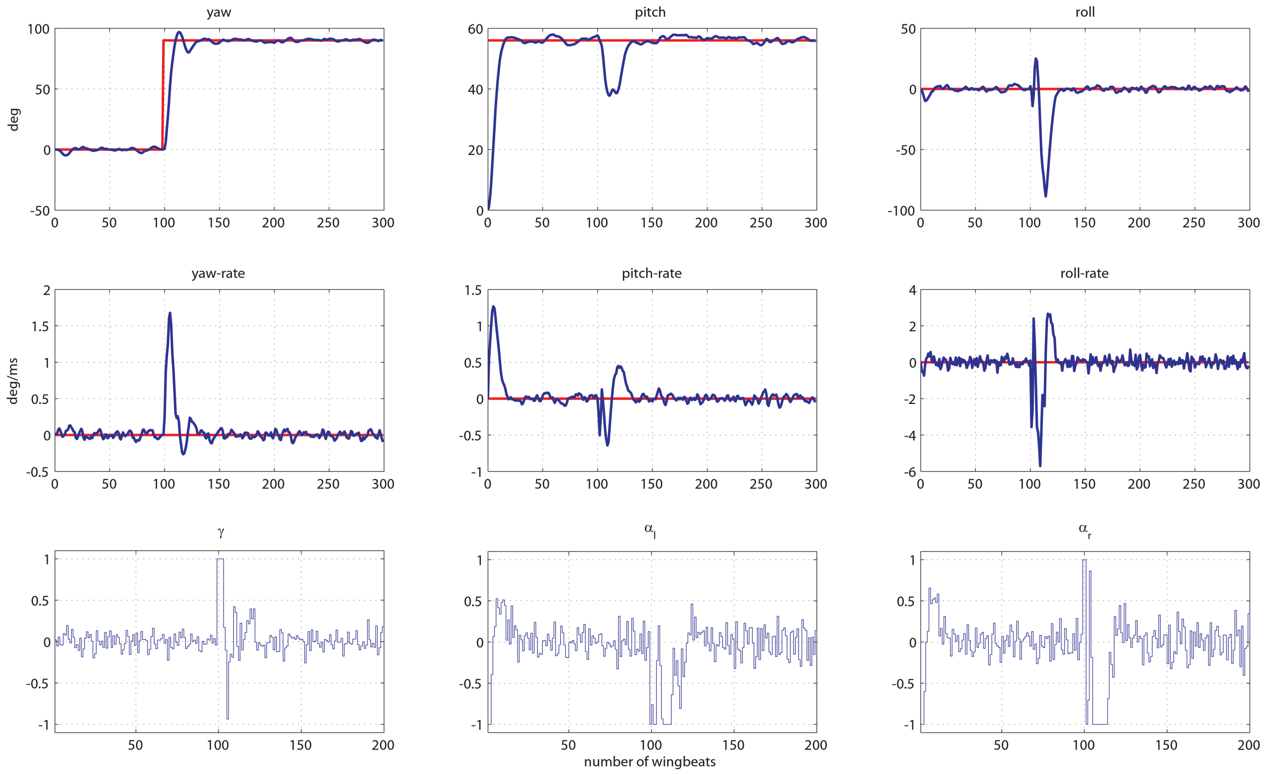

Fig. 6. Tracking saccadic turning in the honey bee model.

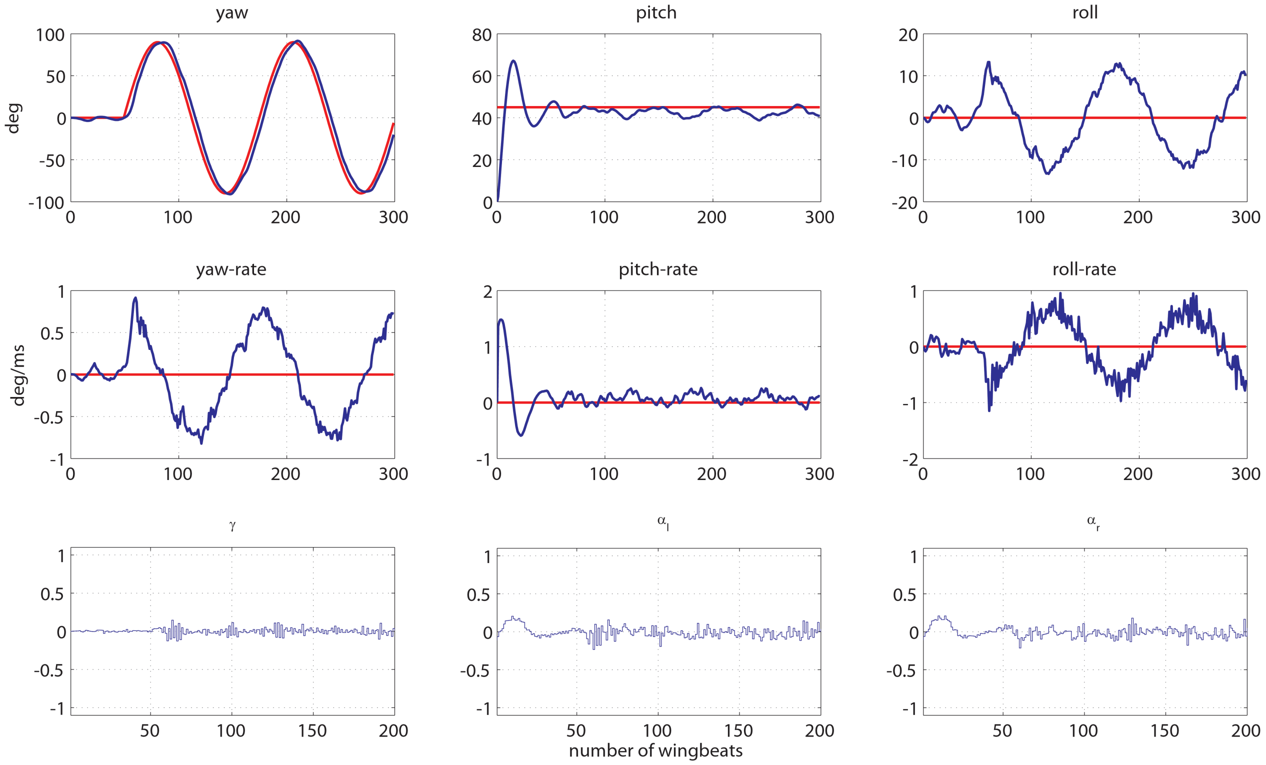

Fig. 7. Tracking sinusoidal yaw variation in the fruit fly model.

as sufficiently large K is selected (without considering saturation in the change of wing kinematic parameters, e.g., maximum ν allowed), a single PD controller also achieves the above tracking tasks without the addition of NN approximation.

5. Conclusions and Future Works

In this paper, we have presented a filtered-error based controller for attitude stabilization and tracking in flapping flight. Nonlinear terms in the dynamic equation have

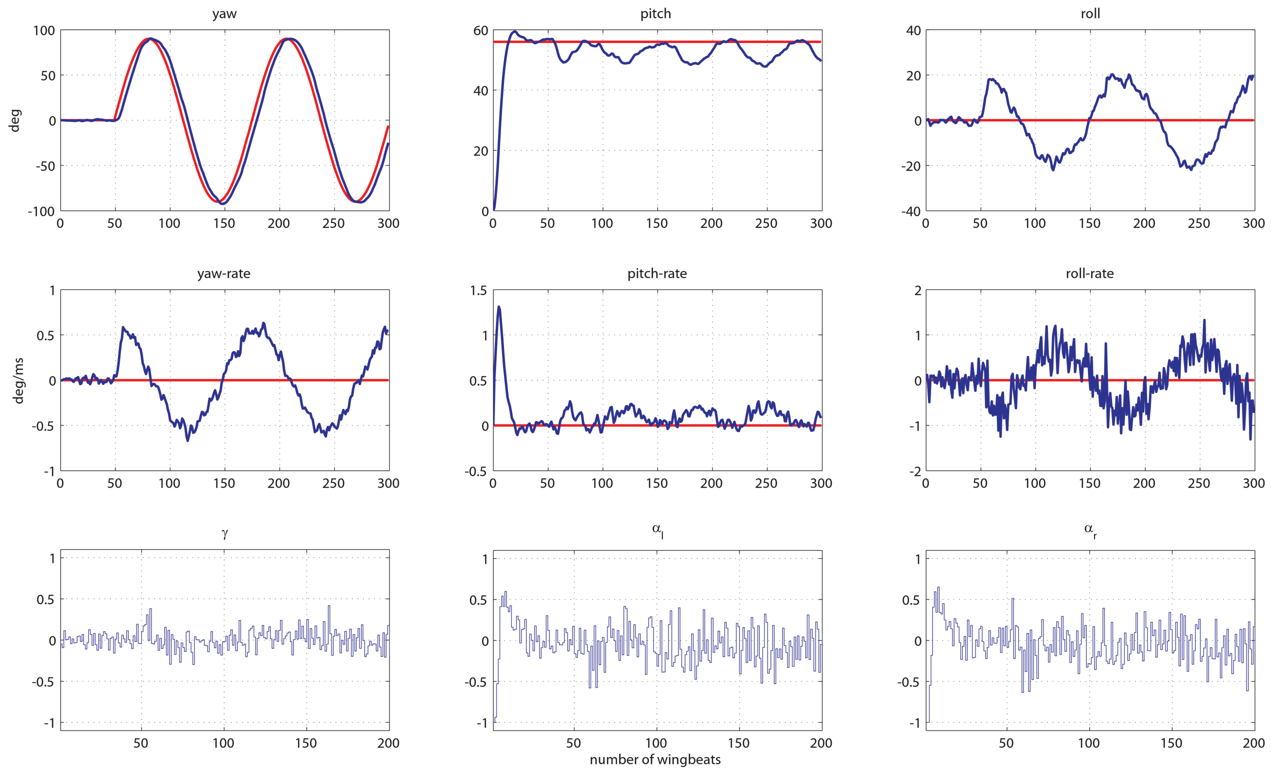

Fig. 8. Tracking sinusoidal yaw variation in the honey bee model.

been approximated by a one-layer FLNN. The controller has successfully achieved stabilization and tracking tasks for two different insect models. Compared to a Linear Quadratic Gaussian (LQG) controller designed solely for stabilization purposes [10], the current controller achieves faster convergence and a broader stable region. In future works, we plan to develop a controller for a complete 6DOF dynamics that is able to achieve stabilization and tracking for both linear and angular body positions. It is also important that we explore additional kinematic parameters increasing the linearity of the aerodynamic mapping $\mathscr{A}(\cdot)$, which possibly reduces the error and nonlinearity in the controller design.

References:

[1] T. S. Collett and M. F. Land, "Visual control of flight behaviour in the hoverfly Syritta pipiens L," J. of Comparative Physiology A: Neuroethology, Sensory, Neural, and Behavioral Physiology, Vol.99, pp. 1-66, 1975.

[2] S. N. Fry, R. Sayaman, and M. H. Dickinson, "The aerodynamics of free-flight maneuvers in Drosophila," Science, Vol.300, pp. 495-498, 2003.

[3] S. N. Fry, R. Sayaman, and M. H. Dickinson, "The aerodynamics of hovering flight in Drosophila," J. of Experimental Biology, Vol.208, pp. 2303-2318, 2005.

[4] G. K. Taylor and A. L. R. Thomas, "Dynamic flight stability in the desert locust Schistocerca gregaria," J. of Experimental Biology, Vol.206, pp. 2803-2829, 2003.

[5] J. A. Bender and M. H. Dickinson, "Comparison of visual and haltere-mediated feedback in the control of body saccades in Drosophila melanogaster," J. of Experimental Biology, Vol.209, pp. 4597-4606, 2006.

[6] M. H. Dickinson, "The initiation and control of rapid flight maneuvers in fruit flies," Integrative and Comparative Biology, Vol.45, pp. 274-281, 2005.

[7] R. Dudley, "The biomechanics of insect flight," Princeton University Press, 2000.

[8] M. H. Dickinson, F. O. Lehmann, and S. P. Sane, "Wing rotation and the aerodynamic basis of insect flight," Science, Vol.284, pp. 1954-1960, 1999.

[9] S. P. Sane and M. H. Dickinson, "The aerodynamic effects of wing rotation and a revised quasi-steady model of flapping flight," J. of Experimental Biology, Vol.205, pp. 1087-1096, 2002.

[10] X. Y. Deng, L. Schenato, and S. S. Sastry, "Flapping flight for biomimetic robotic insects: Part II – Flight control design," IEEE Trans. on Robotics, Vol.22, pp. 789-803, 2006.

[11] X. Y. Deng, L. Schenato, W. C. Wu, and S. S. Sastry, "Flapping flight for biomimetic robotic insects: Part I – System modeling," IEEE Trans. on Robotics, Vol.22, pp. 776-788, 2006.

[12] W. B. Dickson, A. D. Straw, C. Poelma, and M. H. Dickinson, "An Integrative Model of Insect Flight Control," AIAA Aerospace Sciences Meeting and Exhibit, Reno, Nevada, 2006.

[13] B. Cheng and X. Deng, "Mathematical Modeling of Near-hover Insect Flight Dynamics," ASME DSCC Dynamic Systems and Control Conf., Cambridge, Massachusetts, 2010.

[14] B. Cheng and X. Deng, "Translational and Rotational Damping of Flapping Flight and Its Dynamics and Stability at Hovering," IEEE, Trans. on Robotics, Vol.27, 2011.

[15] B. Cheng and X. Deng, "Near-Hover Dynamics and Attitude Stabilization of an Insect Model," in American Control Conf., Baltimore 2010.

[16] B. Cheng, X. Deng, and T. L. Hedrick, "The Mechanics and Control of Pitching Manoeuvres in a Freely Flying Hawkmoth (Manduca Sexta)," J. of Experiment Biology, Vol.214, pp. 4092-4106, 2011.

[17] A. J. Bergou, L. Ristroph, J. Guckenheimer, I. Cohen, and Z. J. Wang, "Fruit Flies Modulate Passive Wing Pitching to Generate In-Flight Turns," Physical Review Letters, Vol.104, p. 148101, 2010.

[18] M. Sun and J. K. Wang, "Flight stabilization control of a hovering model insect," J. of Experimental Biology, Vol.210, pp. 2714-2722, 2007.

[19] F. L. Lewis, S. Jagannathan, and A. Yesildirek, "Neural network control of robot manipulators and nonlinear systems," Philadelphia: Taylor & Francis, 1999.

[20] S. Haykin, "Neural Networks: A Comprehensive Foundation," Macmillan College Publishing Company, 1994.

[21] L. Schenato, X. Deng, W. C. Wu, and S. Sastry, "Virtual insect flight simulator (VIFS): a software testbed for insect flight," Proc. of the IEEE Int. Conf. on Robotics and Automation, Vol.4, pp. 3885-3892, 2001.

[22] R. M. Murray, Z. Li, and S. S. Sastry, "A Mathematical Introduction to Robotic Manipulation," CRC, 1994.

[23] S. P. Sane and M. H. Dickinson, "The control of flight force by a flapping wing: lift and drag production," J. of Experimental Biology, Vol.204, pp. 2607-2626, 2001.

[24] G. K. Taylor, "Mechanics and aerodynamics of insect flight control," Biological Reviews, Vol.76, pp. 449-471, 2001.

[25] S. Mao and X. Yan, "Dynamic flight stability of a hovering bumblebee," J. of Experimental Biology, Vol.208, pp. 447-459, 2005.

[26] X. Deng, L. Schenato, and S. Sastry, "Model Identification and Attitude Control for a Micromechanical Flying Insect Including Thorax and Sensor Models" Proc. of the IEEE Int. Conf. on Robotics & Automation, Taipei, Taiwan, pp. 1152-1157, 2003.

[27] X. Deng, L. Schenato, and S. Sastry, "Model Identification and Attitude Control Scheme for a Micromechanical Flying Insect," Seventh Int. Conf. on Control, Automation, Robotics And Vision (ICARCV '02), Singapore, pp. 1007-1012, 2002.

[28] R. Dudley and C. P. Ellington, "Mechanics of Forward Flight in Bumblebees: I. Kinematics and Morphology," J. of Experimental Biology Vol.148, pp. 19-52, 1990.

Name:
Bo Cheng

Affiliation:
School of Mechanical Engineering, Purdue University

Address:
585 Purdue Mall, West Lafayette, Indiana 47907-2088, USA

Brief Biographical History:

2006 Received B.S. degree in Automation from Zhejiang University, Hangzhou, China

2009 Received M.S. degree in Mechanical Engineering from the University of Delaware, Newark

2009- Ph.D. Student, School of Mechanical Engineering, Purdue University

Main Works:

- aerodynamics, modeling of dynamics and control in flapping-wing flight, designing of biomimetic micro air vehicles

Name:
Xinyan Deng

Affiliation:
School of Mechanical Engineering, Purdue University

Address:
585 Purdue Mall, West Lafayette, Indiana 47907-2088, USA

Brief Biographical History:

1995 Received B.S. degree in Automation from Tianjin University

2004 Received Ph.D. degree in Mechanical Engineering from the University of California, Berkeley

2004-2009 Assistant Professor, Department of Mechanical Engineering, the University of Delaware

2009- Assistant Professor, School of Mechanical Engineering, Purdue University

Main Works:

- dynamics and aerodynamics in flapping flight, bio-inspired robots, micro air vehicles, underwater vehicles